Real-time and non-invasive measurements of cell mechanical behaviour with optical coherence phase microscopy

Real-time and non-invasive measurements of cell mechanical behaviour with optical coherence phase microscopy

D Gillies[1,2], W Gamal[2], A Downes[2], Y Reinwald[3], Y Yang[3], A El Haj[3], P O Bagnaninchi[1*]

[1]MRC Scottish Centre for Regenerative Medicine, The University of Edinburgh, Edinburgh, UK

[2]Institute for Bioengineering, School of Engineering, The University of Edinburgh, Edinburgh, UK

[3]Institute for Science and Technology in Medicine, Keele University, Keele, UK

*Corresponding Author: Pierre.Bagnaninchi@ed.ac.uk

Abstract

Cell mechanical behaviour is increasingly recognised as a central biophysical parameter in cancer and stem cell research, and methods of investigating their mechanical behaviour are therefore needed.

We have developed a novel qualitative method based on quantitative phase imaging which is capable of investigating cell mechanical behaviour in real-time at cellular resolution using Optical Coherence Phase Microscopy (OCPM), and stimulating the cells non-invasively using hydrostatic pressure. The method was exemplified to distinguish between cells with distinct mechanical properties, and transient change induced by Cytochalasin D.

We showed the potential of quantitative phase imaging to detect nanoscale intracellular displacement induced by varying hydrostatic pressure in microfluidic channels, reflecting cell mechanical behaviour. Further physical modelling is required to yield quantitative mechanical properties.

Keywords: optical coherence phase microscopy, mechanical behaviour, real-time monitoring, hydrostatic pressure, phase imaging

1. Introduction

There are more than fifteen cancer deaths per minute globally [1], with over 90% of cancer deaths caused by metastasis [2]. Metastasis is known to alter the mechanical behaviour of cells from the nanoscopic to macroscopic scales [3], with metastatic potential increasing as cell stiffness decreases [4 - 7], and nanoscale features of synthetic surfaces have been shown to influence cell behaviour [8].

Similarly, stem cells are vitally important in regenerative and therapeutic medicine due to their self-renewal and differentiation abilities. Mechanical stimuli have been shown to have a major role in regulating stem cell behaviour, with differentiation controlled by the stiffness of the substrate where stem cells attach, through a mechanosensitive process [9]. Therefore, there is a clear need to investigate the mechanical behaviour of cancer cells and stem cells as well as their response to various mechanical stimuli.

Clinicians have used manual palpation of suspect tissues as a qualitative diagnostic tool for centuries. It is, however, subjective, and carried out on the macroscopic scale. Non-invasive imaging techniques such as ultrasound and Magnetic Resonance Imaging (MRI) elastography have translated to the clinic [10, 11], however both lack the spatial resolution to be used on the cellular scale. The measurement of mechanical behaviour on the nano- and microscopic scale has used techniques such as atomic force microscopy (AFM), optical tweezers, and optical coherence elastography (OCE) [12, 13]. These do, however, suffer from drawbacks for single cell characterisation in that they use contact loading or are

unable to assess cellular mechanics in a 3D microenvironment. Still, AFM is one of the most common techniques currently available to assess cell mechanics [14-16]. It uses a cantilever and tip to determine quantitative cell mechanical properties, achieving high resolution and mechanical sensitivity, but is inherently invasive, and as a surface-based technique it cannot investigate intracellular mechanical properties or when cells are cultured in a 3D environment.

Consequently, optical techniques to investigates cell mechanics are rapidly emerging and are reviewed in [13]. Optical coherence tomography (OCE) maps the mechanical properties of tissue by detecting the depth-resolved deformation produced as a result of compression [13, 20-22]. It is an extension of OCT, a low-coherence interferometry based imaging technique which uses the optical scattering properties of a sample in a manner analogous to ultrasound to create either a 2-D or 3-D image which shows structural features at the micrometer scale [17-19]. OCE is comparable to palpation in that a force is applied to the sample under investigation and the resulting displacement tracked [3]. To date, OCE systems typically achieve a depth of focus of 0.5 – 3 mm and A-scan rate greater than 20 kHz [13, 22].

Combining OCT with high transverse resolution confocal microscopy results in optical coherence microscopy (OCM), achieving sub-micron resolution imaging with high dynamic range and sensitivity, allowing for 3D cellular imaging. OCM further extends to Optical Coherence Phase Microscopy (OCPM), a quantitative phase imaging method, to measure the phase changes and cross-sectional depth information from a sample. As such OCPM is part of a range of label-free optical microscopy techniques known as Quantitative phase imaging (QPI) [23, 24] which uses the phase contrast of a sample to improve upon intrinsic contrast imaging. The shift in optical path length (OPL) created by the sample is measured quantitatively at the nanometre scale. It is a powerful label-free tool which has been used to investigate the biophysics of red blood cells [25, 26], cell growth [27], and track microbial motility [28].

OCPM is sensitive to sub-micrometer changes in OPL, and achieves high spatial resolution. It is therefore an ideal candidate for monitoring displacements. OCPM has been used to characterise nanoscale cellular dynamics in live cells [29], and has been shown to measure cell viability based on intracellular optical fluctuations [30, 31].

In this study, we aimed to propose a method for the contact-less assessment of cell mechanical behaviour in vitro that will allow further longitudinal studies without damaging the cells or compromising cell culture sterility. Therefore, we described a novel method based on a standard commercial OCT that can measure the relative cell mechanical response to hydrostatic pressure non-invasively and in real-time. This method will be easily translatable to any spectral domain OCT and with some modifications to most of the QPI methods.

2. Materials and Methods

2.1 Cell culture

Breast cancer cells (MCF-7) and mouse fibroblasts (3T3) were used in this study to provide two lineages with distinct mechanical properties. Both were cultured in Dulbecco's Modified Eagle Medium (DMEM) with 10% foetal bovine serum, 1% L-glutamine and 1% Penicillin-Streptomycin. Cells were incubated at 37^0C and 5% CO_2 and were passaged every 3 days. Cells were dissociated using trypsin-EDTA and transferred to microfluidic channels (microslide IV, Ibidi) 24 hours prior to experimentation. We used adherent cells lines that attached to the bottom substrate of the channels.

2.2 Hydrostatic Force

In this study, we modulated the hydrostatic pressure in microfluidic channels to induce a hydrostatic force on adherent cells attaching at bottom surface of the channels to produce a non-contact force similar to previous work [32]. In this work, we used controlled cyclic square wave pressure, instead of a pressure column. We generated a change in hydrostatic pressure in the microfluidics channels by altering the air pressure in a fluid container (falcon, 50mL), connected through a Tygon (Saint-Gobain, France) tube to microfluidic channels (microslide IV, Ibidi).

In first approximation, we can consider the cells as half-spheres attached to an incompressible solid substrate (see figure 1). Pressure and force are transmitted equally to all directions, and on figure 1 we will have equal forces on the right and left side of the cell, with no net horizontal hydrostatic component. Whereas there will be a net vertical force, F_v, at the top of the cell proportional to the projected area. For a cell of radius r, we have:

$$F_v = (\Delta P + \rho g h)(\pi r^2) + \rho g V_w \qquad (1)$$

Where $\triangle P$ is the applied pressure change above the atmospheric pressure, ρ is the water density (1000 kgm^{-3}), h the height of the water column, and g the gravitational acceleration (9.81 ms^{-2}). V_w is the volume of water on top of the cell starting from the cell top. It can be written as the difference between the cell volume and the volume of an imaginary rectangular box surrounding the cell.

$$V_w = 8r^3 - (4/6)\pi r^2 \qquad (2)$$

Typically for a cell of radius 20 μm and $\triangle P$=1000 $N.m^{-2}$ (10 mbar) we calculated a net vertical force of 1.2 μN. We would like to point out that this framework approximated the cross-sectional area as related to cell diameter whereas cells contact the substrate through focal point. This could lead to acting net vertical force an order of magnitude lower, i.e. in the nano-Newton range. Nonetheless, this showed that an actual force is exerted on the cells due to both the hydrostatic pressure and the presence of an underlying substrate.

In this study, MCF-7 and 3T3 cells were exposed to cyclic mechanical stimuli in the form of square wave hydrostatic pressure from a microfluidic pressure pump (AF1, Elveflow, France), inside a microfluidic channel with pressure ranging from 1000 Nm^{-2} to 20000 Nm^{-2} with frequencies ranging from 80-300 mHz. It was ensured that no air bubbles were present in the sample medium by allowing a flow of media through the microchannel before sealing with a Luer lock plug (Elveflow, France).

2.3 Optical coherence phase microscopy

Experimental setup

The OCPM system was based around a commercial Thorlabs Callisto optical coherence tomography (OCT) system, as shown in figure 2. The superluminescent light source was centred at 930 nm with a full width half maximum (FWHM) of 90 nm, with an axial resolution of 5um in water. The scanning rate is 1.2KHz; which was order of magnitude lower than state of the art OCT used for OCE. The light source was output to a FC/APC fibre, which is the guided with an F280APC-B collimating lens (Thorlabs, NJ, USA). The light path is then directed by galvanometers which control the image acquisition, and finally is coupled into the side port of a Leica DMIRE2 microscope. The system is built in a common path configuration to improve the phase stability [33]. Using a beamsplitter (Thorlabs, NJ, USA), the

brightfield image of the sample was collected digitally using a CMOS camera (Thorlabs, NJ, USA). A full list of components can be found in section 6.

The acquired spectra were then processed as described in figure 3. First, the average background was removed, then the signal is resampled in k-space. The modulation of the spectra, collected at a spatial location x_i,y_i, encodes the in-depth location (z_i) of the scattering particles, which are retrieved by zero-padding of the signal and fast Fourier transform. This forms the A-scan at the location (x_i,y_i) and the real part [35] of the complex signal is compressed on a log scale to give a depth-dependent intensity profile; while the phase at each depth z_i of the OCT signal is retrieved from the argument.

2.4 Quantifying intracellular displacement due to cyclic hydroforce

A 4D data cube (256x256x512x96 in x, y, z, t pixels) was captured with an acquisition frequency of 1,200 A-scans, or (x, z) scans, per second to sample the varying phase over time. A quantitative measurement of the change in phase was calculated as the differing phase between successive B-scans. Therefore, the phase was unwrapped along the time-dimension and not spatially. This was implemented directly with the Matlab (Mathworks) function unwrap.

The phase difference was then converted into displacement, d, through the following equation:

$$d = \frac{\Delta\Phi\lambda_0}{4\pi n} \qquad (3)$$

Where; n is the refractive index, λ_0 is the central wavelength and $\Delta\Phi$ is the phase difference between adjacent B scans. In OCPM, the phase stability is defined as the square root of the phase variance, which is inversely related to the SNR [33]. With a theoretical SNR of 83 dB in air, the system had a theoretical phase stability of $7e^{-5}$ radians [34]. In liquid medium, the SNR was measured as 35 dB corresponding to a phase resolution of 0.01 radian [31].

For rectangular input pressure, the relative displacement of each pixel, Δd, was then determined through the equation:

$$\Delta d = 2 * \Delta\Phi \; RMS(x, y) \frac{\lambda_0}{4\pi n} \qquad (4)$$

Where; $\Delta\Phi$RMS(x, y) is the root mean squared (RMS) phase change at each pixel as a result of the induced displacement. This gives us a qualitative measurement of the cell mechanical behaviour in response to hydrostatic pressure.

Our experimental set-up achieves a scan rate adequate for acquiring the mechanical behaviour of cultured cells. Whilst the scan rate used in our system is lower than the current state of the art, this method is easily translatable to other systems where a higher rate could be used.

2.5 Assessing whole cell response

To assess the whole cell mechanical qualitative behaviour, we plotted the distribution of the relative displacement ass calculated in (4) all pixels within the cell, and analysed their distribution. Pixels belonging to a cell were determined by first, manually removing the first strong reflections associated with the plastic substrate, and then using an intensity-based mask to delineate the cells.

2.5 Cellscale Microsquisher®

In order to confirm an appropriate optical phantom for the OCPM set-up in term of both its optical and mechanical properties, 6% (w/v) agarose beads (Agarose bead technology, Madrid, Spain) of diameter 150 µm to 350 µm were subjected to parallel plate compression in a water bath at a strain rate of 2.5 μms^{-1} using the Cell Scale Microsquisher® and results recorded in the associated Squisherjoy software. A 1 mm compression plate was attached to a 235 µm microbeam. The force vs displacement data was then converted into stress vs strain data, with the associated curve used to obtain a linear regression line from which the elasticity was calculated at 10% nominal compression of the sphere.

Theory

Force vs displacement data was converted to stress vs strain using a modified Hertz model [35] as described below.

$$\Phi = cos^{-1}\left(\frac{R-\delta}{R}\right) \quad (5)$$

$$a = (R-\delta)tan\Phi \quad (6)$$

$$f(a) = \frac{2(1+v)R^2}{(a^2+4R^2)^{3/2}} + \frac{1-v^2}{(a^2+4R^2)^{1/2}} \quad (7)$$

$$E = \frac{3(1-v^2)F}{4\delta a} - \frac{f(a)F}{\pi\delta} \quad (8)$$

Where; F is the applied force, R is the sphere radius, δ is the displacement, v the Poisson's ratio (0.5) and E the Young's Modulus.

3. Results and Discussion

In this paper, we presented an optical coherence elastography method in which the novelty relied mostly on the way the mechanical forces were realised in a non-contact way to allow live cell measurement, and on the associated signal processing techniques. We demonstrated, and exemplified for single pixels in figure 7, that this method created intracellular displacements within the cells that were directly coupled to the input mechanical stimuli, and that they were correlated to transient changes in cell mechanical properties after addition of Cytochalasin D, and that they could distinguish two exemplar cell line extensively studied for their mechanical properties. The proposed optical set-up was based on a commercial OCT engine (Callisto, Thorlabs) with relatively low specification when compared to recent advances in the field [13], and could therefore translated easily to higher specifications OCT systems and with some small modification to most of the QPI techniques.

Figure 5 (a) shows the stress-strain curve of 6% agarose beads (Agarose bead technology, Madrid, Spain) acquired from plate to plate compression tests using the Cell Scale Microsquisher system, shown in (b). This was converted from force-displacement to stress strain using the modified Hertz model described in section 2.5. The mean Young's modulus was determined to be 834 Pa ± 45 Pa at 10% nominal compression of the bead. Single beads of varying diameter from 150-350 µm were tested in a water bath. This helped us to confirm that the mechanical properties of agarose beads were in the same order of magnitude as of biological cells that typically range in the 1 kPa region [5]. They were therefore a well calibrated test sample to test the new methods based on OCPM.

In figure 6 we report the mean intensity map (a) and phase response (b)-(d) of agarose beads of size 150-350 µm, measured using the novel OCPM system. The period of a 100 mbar hydrostatic pressure

was varied, with the phase response to 4 s, 6 s, and 12 s cycles shown in figure 6 (b), (c), and (d) respectively at one pixel of the bead. The change in the time varying phase response correlated directly to the change in pressure cycle. This demonstrated that OCPM could monitor nanoscale displacements induced by hydrostatic pressure in materials with mechanical properties comparable to biological cells; and could therefore be used to map the relative mechanical properties of cells in a non-invasive and real-time manner.

We then used the OCPM system to measure the mechanical behaviour of MCF-7 cells in response to varying hydrostatic pressure (figure 7), where we plot the response of a single pixel of the cell under test. Here we show a bright field image of the MCF-7 cells in (a) with the corresponding OCPM en-face image and OCPM B-scan or 'cell profile' in figure 7 (b) and (c). Cyclic stress was successfully applied directly to cells within the microfluidic chip and the corresponding displacement was recorded in real-time at the nanometre scale for each pixel of the cell (see figure 7 (d)-(k)). A change in amplitude and/or frequency of the stimuli was translated to a corresponding cell response.In (d), (e) and (f) the amplitude was varied, with the phase response of a single pixel within the cell to 0, 100, and 200mbar cycles of 6s shown respectively. Here we see a clear change in the phase response which is directly proportional to the change in stimulus. In (g), (h) and (i) we show the phase response to a variation in the period of the cyclic stress. The response to 4, 6, and 12s cycles at an amplitude of 200mbar are shown here. Again, we can see that the response clearly correlates to the change in stimulus.

Note that Intra-cellular variability in local biomechanical properties gives rise to some variation in the amplitude of the response when comparing different pixel at same amplitude (figure 7(f) and (h)). To account for this whole cell mechanical response should be assessed as described in section 2.5 and not based on selected pixel values.

We then looked at the ability of the system to monitor the relative biomechanical properties of cells known to be of different stiffness. In (j) we show the phase response of MCF-7 cells to 50mbar of pressure with a 6s period. We then exposed the cells to 10µM Cytochalasin-D, an actin polymerisation inhibitor known to reduce cell stiffness [36], for 180 minutes prior to recording the phase response in (k). We can see an increased response here, indicating that the cells were indeed softer after the addition of Cytochalasin-D. We then calculated the mean RMS of the phase signal in (l) for all pixels of the cell. This gives a quantitative comparison of the relative cell response which confirms that the cells were indeed significantly softer as expected after exposure to the drug ($p<0.01$), demonstrating the potential of OCPM combined with hydrostatic pressure to monitor non-destructively and in real-time cell mechanical behaviour.

In figure 8 we compare two cell lines with distinctly different mechanical properties. We compare the properties of 3T3 cells with MCF-7 cells. 3T3 cells have previously been described as stiffer that MCF-7 in [4]. In (a) we show an en-face image of MCF-7 cells, and of 3T3 in (d). Interferences between the reflections from the cell membrane and the glass surface generates "spatial" coherent interference fringes in intensity when the cell thickness is below the coherence gate (<5µm in this case), hence the banding effect observed in (d). These fringes were, however, not detrimental to our method as phase differences were calculated along the time dimension (successive B scans), and not adjacent pixels. We show B-scans, or 'cell profiles' of MCF-7 and 3T3 in (b) and (e) respectively, and the corresponding mechanical contrast maps of relative displacement in (c) and (f), where the relative displacement increases as the map moves to yellow.

This map is quantified in (g) and (h) where we plot the relative displacement for all pixels in the cell on a histogram. It is quite clear from this that the mean displacement of the MCF-7 cells is much greater than that of the 3T3, showing a marked difference in the relative displacement between

different cell lines. The high level of mean displacement recorded for MCF-7 cells indicates a soft cell, with the low mean displacement if 3T3 indicating a stiffer cell. This data agrees with the figures previously reported in literature, which state that 3T3 cells are stiffer [37, 4].

This evidence indicates that this novel non-destructive method is capable of providing a qualitative description of cell mechanical behaviour, and map of mechanical contrast. Qualitative mechanical contrast has been shown as a clinically relevant method in [38-43].

4. Conclusions

We have described a new qualitative method, based on the principles of quantitative phase imaging, to monitor in real-time and non-destructively the mechanical behaviour of cells in monolayers that is directly translatable to the study of the mechanical behaviour of cancer cells and of the stem cell niche.

The novelty of this proof-of-principle method relied on the way the mechanical forces were realised in a non-contact way to allow live cell measurement, and on the associated signal processing techniques. We showed that we could generate and measure intracellular displacements within the cells that were directly coupled to the input mechanical stimuli. And, that these recorded changes in phase were correlated to transient changes in cell mechanical properties after addition of Cytochalasin D. Finally, we proposed a method to study intracellular displacement for whole cell that could distinguish two exemplar cell line extensively studied for their mechanical properties

5 Acknowledgements

The authors are grateful to the research group of Dr Anthony Callanan in the Institute for BioEngineering, University of Edinburgh, Edinburgh, UK for facilitating use of the Cell Scale Microsquisher® system.

This work was supported by the School of Engineering, University of Edinburgh and the Engineering and Physical Sciences Research Council and Medical Research Council [grant number EP/L016559/1], and the UKRMP Engineering and exploiting the stem cell niche hub [grant number MR/K026666/1].

6 Supplier list

Hydrostatic Pressure

Hydrostatic pressure pump	AF1	Elveflow, France
Falcon tube medium accessory kit	50ml	Elveflow, France
Microfluidic channel	Microslide VI	Ibidi, Germany

Optical Coherence Phase Microscopy

OCT system	Callisto	Thorlabs, NJ, USA
Microscope	DMIRE2	Leica, Germany
2D Galvo system, silver coated mirrors	GVS002	Thorlabs, NJ, USA
2D Galvo system linear power supply	GPS011	Thorlabs, NJ, USA
30mm cage compatible smooth bore kinematic mount	KC1	Thorlabs, NJ, USA
F=50mm 1” mounted achromatic doublet, SM1 thread-mount, ARC: 650-1050nm	AC254-050-B-ML	Thorlabs, NJ, USA
30mm Cage cube-mounted non-polarizing beamsplitter, 700-1100nm, M4 Tap	CCM1-BS014/M	Thorlabs, NJ, USA
Fibre collimation package	F280APC-B	Thorlabs, NJ, USA
SM1 threaded adapter	AD11F	Thorlabs, NJ, USA

Cellscale Microsquisher

Micro scale tension compression test system	Microsquisher	Cellscale, ON, Canada
Microbeam cantilever	203.2nm	Cellscale, ON, Canada
Compression plate	1mm x 1mm	Cellscale, ON, Canada

7 References

[1] B. W. Stewart, C. P. Wild, World cancer report 2014, IARC Press, Lyon, 2014

[2] C. L. Chaffer, R. A. Weinberg, A perspective on cancer cell metastasis, Science 331(6024), 1559-1564(2011)

[3] B. F. Kennedy, K. M. Kennedy, D. D. Sampson, A Review of Optical Coherence Elastography: Fundamentals, Techniques, and Prospects, IEEE J. Sel. Topics Quantum Electron. 20(2), 272-288(2014)

[4] J. Rother, H. Nöding, I. Mey, A. Janshoff, Atomic force microscopy-based microrheology reveals significant differences in the viscoelastic response between malign and benign cell lines, Open Biol. 4(5), 140046(2014)

[5] M. Plodinec, M. Loparic, C. A. Monnier, E. C. Obermann, R. Zanetti-Dallenbach, P. Oertle, J. T. Hyotyla, U. Aebi, M. Bentires-Alj, R. Y. H. Lim, C. Schoenberger, The nanomechanical signature of breast cancer, Nat. Nanotechnol. 7(11), 757-756(2012)

[6] W. Xu, R. Mezencev, B. Kim, L. Wang, J. McDonald, T. Sulchek, Cell stiffness is a biomarker of the metastatic potential of ovarian cancer cells, PLos One 7(10), e46609(2012)

[7] Z. Zhou, C. Zheng, S. Li, X. Zhou, Z. Liu, Q. He, N. Zhang, A. Ngan, B. Tang, A. Wang, AFM nanoindentation detection of the elastic modulus of tongue squamous carcinoma cells with different metastatic potentials, Nanomedicine 9(7), 864-874(2013)

[8] E. K. F. Kim, E. M. Darling, K. Kulangara, F. Guilak, K. W. Leong, Nanophotography-induced changes in focal adhesions, cytoskeletal organisation, and mechanical properties of human mesenchymal stem cells, Biomaterials 31(6), 1299-1306(2010)

[9] A. J. Engler, S. Sen, H. L. Sweeney, D. E. Discher, Matrix elasticity directs stem cell lineage specification, Cell 126(4), 677-89(2006)

[10] K. J. Glaser, A. Manduca, R. L. Ehman, Review of MR elastography applications and recent developments, J. Magn. Reson. Imaging 36(4), 757-774(2012)

[11] R. M. S. Sigrist, J. Liau, A. E. Kaffas, M. C. Chammas, J. K. Willmann, Ultrasound elastography: review of techniques and clinical applications, Theranostics 7(5), 1303-1329(2017)

[12] B. F. Kennedy, R. A. McLaughlin, K. M. Kennedy, A. C. Chin, A. Tien, B. Latham, C. B. Saunders, D. D. Sampson, Optical coherence micro-elastography: mechanical-contrast imaging of tissue microstructure, Biomed. Opt. Express 5(7), 2113-2124(2014)

[13] B. F. Kennedy, P. Wijesinghe, D. D. Sampson, The emergence of optical elastography in biomedicine, Nat. Photon 11, 215-221(2017)

[14] G. Binnig, C. F. Quate, C. Gerber, Atomic force microscope, Phys. Rev. Lett. 56(9), 930-933(1986)

[15] M. Radmacher, R. W. Tillamnn, M. Fritz, H. E. Gaub, From molecules to cells: imaging soft samples with the atomic force microscope, Science 257(5078), 1900-1905(1992)

[16] D. Tsikritsis, S. Richmond, P. Stewart, A. Elfick, A. Downes, Label-free identification and characterisation of living human primary and secondary tumour cells, Analyst 140(15), 5162-5168(2015)

[17] D. Huang, E. A. Swanson, C. P. Lin, J. S. Schuman, W. G. Stinson, W. Chang, M. R. Hee, T. Flotte, K. Gregory, C. A. Puliafito, J. G. Fujimoto, Optical Coherence Tomography, Science 254(5035), 1178-1181(1991)

[18] P. H. Tomlins, R. K. Wang, Theory, developments and applications of optical coherence tomography, J. Phys. D: Appl. Phys. 38(15), 2519(2005)

[19] A. M. Zysk, F. T. Nguyen, A. L. Oldenburg, D. L. Marks, S. A. Boppart, Optical coherence tomography: a review of clinical development from bench to bedside, J. Biomed. Opt. 12(5), 051403(2007)

[20] J. M. Schmitt, OCT elastography: imaging microscopic deformation and strain of tissue, Opt. Express 3(6), 199-211(1998)

[21] H. Ko, W. Tan, R. Stack, S. A. Boppart, Optical coherence elastography of engineered and developing tissue, J. Tissue Eng. 12(1), 63-73(2006)

[22] A. Curatolo, M. Villiger, D. Lorenser, P. Wijesinghe, A. Fritz, B. Kennedy, D. D. Sampson, Ultrahigh-resolution optical coherence elastography, Opt. Lett. 41(1), 21-21(2016)

[23] G. Popescu, Quantitative phase imaging of cells and tissues, McGraw-Hill, New York, 2012

[24] M. Mir, B. Bhaduri, R. Wang, R. Zhu, G. Popescu, Quantitative Phase Imaging, Progress in Optics 57, 133-217(2012)

[25] G. Popescu, Y. Park, W. Choi, R. R. Dasari, M. S. Feld, K. Badizadegan, Imaging red blood cell dynamics by quantitative phase microscopy, Blood Cell Mol. Dis. 41(1), 10-16(2008)

[26] Y. Park, T. Yamauchi, W. Choi, R. Dasari, M. S. Feld, Spectroscopic phase microscopy for quantifying haemoglobin concentrations in intact red blood cells, Opt. Lett. 34(23), 3668–3670(2009)

[27] K. Park, L. J. Millet, N. Kim, H. Li, X. Jin, G. Popescu, N. R. Aluru, K. J. Hsia, R. Bashir, Measurement of adherent cell mass and growth, Proc. Natl. Acad. Sci. USA 107(48), 20691–20696(2010)

[28] J. Kühn, B. Niraula, K. Liewer, J. K. Wallace, E. Serabyn, E. Graff, C. Lindensmith, J. Nadeau, A Mach-Zender digital holographic microscope with sub-micrometer resolution for imaging and tracking of marine micro-organisms, Rev, Sci, Instrum. 85(12), 123113(2014)

[29] A. K. Ellerbee, T. L. Creazzo, J. A. Izatt, Investigating nanoscale cellular dynamic with cross-sectional spectral domain phase microscopy, Opt. Express 15(13), 8115-8124(2007)

[30] C. Holmes, M. Tabrizian, P. O. Bagnaninchi, Motility imaging via optical coherence phase microscopy enables label-free monitoring of tissue growth and viability in 3D tissue-engineering scaffolds, J. Tissue Eng. Regen. Med. 9(5), 641-645(2015)

[31] P.O. Bagnaninchi, C. Holmes, N. Drummond, J. Daoud, M. Tabrizian, Two-dimensional and three-dimensional viability measurements of adult stem cells with optical coherence phase microscopy, J. Biomed. Opt. 16(8), 086003(2011)

[32] L. A. G. Lin, A. Q. Liu, Y. F. Yu, C. Zhang, C. S. Lim, S. H. Ng, P. H. Yap, H. J. Gao, Cell compressibility studies utilizing noncontact hydrostatic pressure measurements on single living cells in a microchamber, Appl. Phys. Lett. 92(23), 233901(2008)

[33] K. S. Lee, H. Hur, H. Y. Sung, I. J. Kim, G. H. Kim, Spectrally encoded common-path fibre-optic-based parallel optical coherence tomography, Opt. Lett. 41(18), 4241-4244(2016)

[34] M. V. Sarunic, B. E. Applegate, J. A. Izatt, Real-time quadrature projection complex conjugate resolved Fourier domain optical coherence tomography, Opt. Lett. 31(16), 2426-2428(2006)

[35] K. Kim, J. Cheung, Q. Liu, X. Y. Wu, Y. Sun, Investigation of mechanical properties of soft hydrogel microcapsules in relation to protein delivery using a MEMS force sensor, J. Biomed. Mater. Res. 92(1), 103-113(2010)

[36] W. J. Elldridge, A. Sheinfeld, M. T. Rinehart, A. Wax, Imaging deformation of adherent cells due to shear stress using quantitative phase imaging, Opt. Lett. 41(2), 352-355(2016)

[37] Y. M. Efremov, W. Wang, S. D. Hardy, R. L. Geahlen, A. Raman, Measuring nanoscale viscoelastic parameters of cells directly from AFM force-displacement curves, Sci. Rep. 7, 1541(2017)

[38] T. M. Mutala, P. Ndaiga, A. Aywak, Comparison of qualitative and semiquantitative strain elastography in breast lesions for diagnostic accuracy, Cancer Imaging 16(12), (2016)

[39] C. Pozza, D. Gianfrilli, G. Fattorini, E. Giannetta, F. Barbagallo, E. Nicolai, C. Cristini, G. B. Di Pierro, G. Franco, A. Lenzi, P. S. Sidhu, V. Cantisani, A. M. Isidori, Diagnostic value of qualitative and strain ratio elastography in the differential diagnosis of non-palpable testicular lesions, Andrology 4(6), 1193-1203(2016)

[40] S. Nell, J. W. Kist, T. P. A. Debray, B. de Keizer, T. J. van Oostenvrugge, I. H. M. Borel Rinkes, G. D. Valk, M. R. Vriens, Qualitative elastography can replace thyroid nodule fine-needle aspiration in patients with soft thyroid nodules. A systematic review and meta-analysis, Eur. J. Radiol. 84(4), 652-661(2015)

[41] J. W. Kist, S. Nell, B. de Keizer, G. D. Valk, I. H. M. Borel Rinkes, M. R. Vriens, The role of qualitative elastography in thyroid nodule evaluation: exploring its target populations, Endocrine 50(2), 265-267(2015)

[42] P. N. T. Wells, H. Liang, Medical ultrasound: imaging of soft tissue strain and elasticity, J. R. Soc. Interface 8(64), 1521-1549(2011)

[43]A. E. Kaffas, D. Bekah, M. Rui, J. C. Kumaradas, M. C. Kolios, Investigating longitudinal changes in the mechanical properties of MCF-7 cells exposed to paclitaxel using particle tracking microrheology, Phys. Med. Biol. 58(4), 923-936(2013)

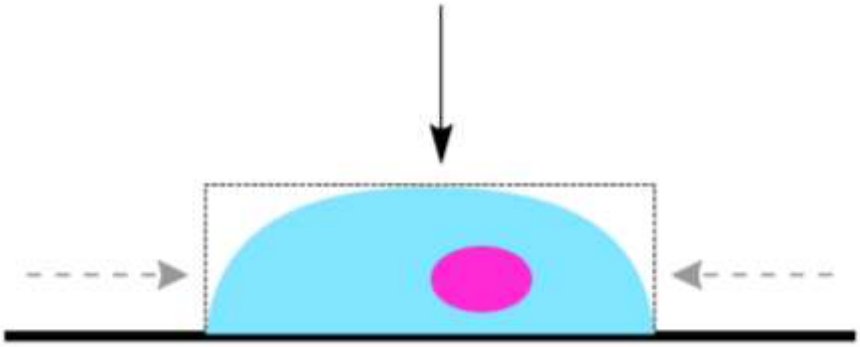

Figure 1: Resulting hydrostatic force induced on adherent cells above a substrate

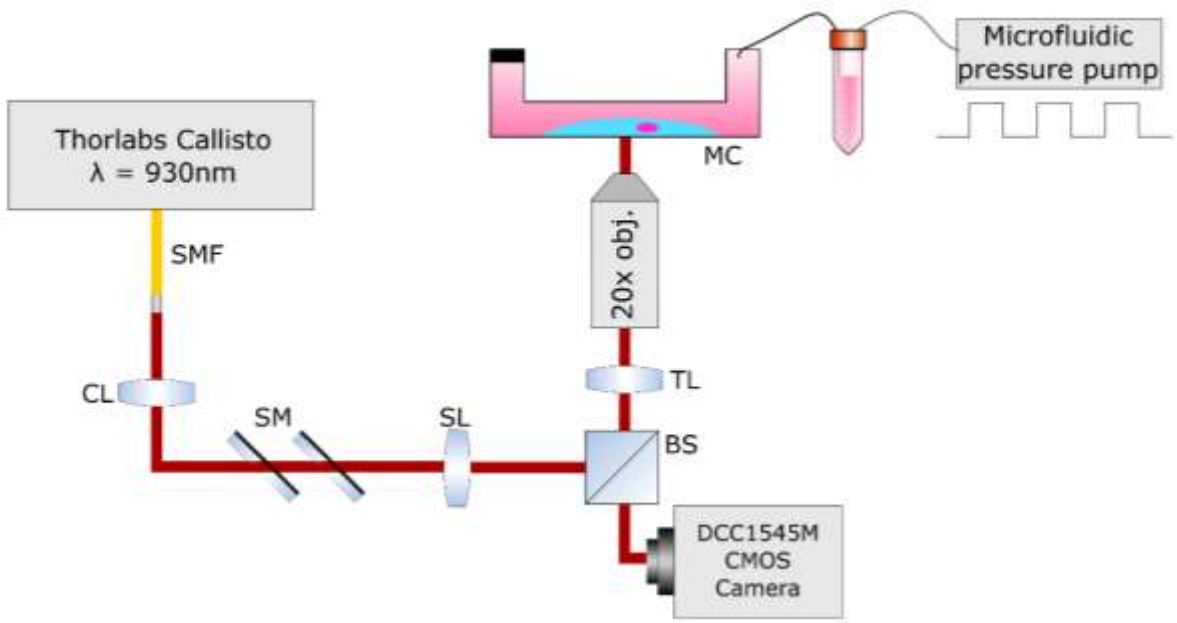

Figure 2: OCPM set-up for qualitative measurement of cell mechanical properties: SMF, single mode fibre; CL, collimating lens; SM, scanning mirrors; SL, scanning lens; BS, beam splitter; TL, tube lens; MC, microchannel.

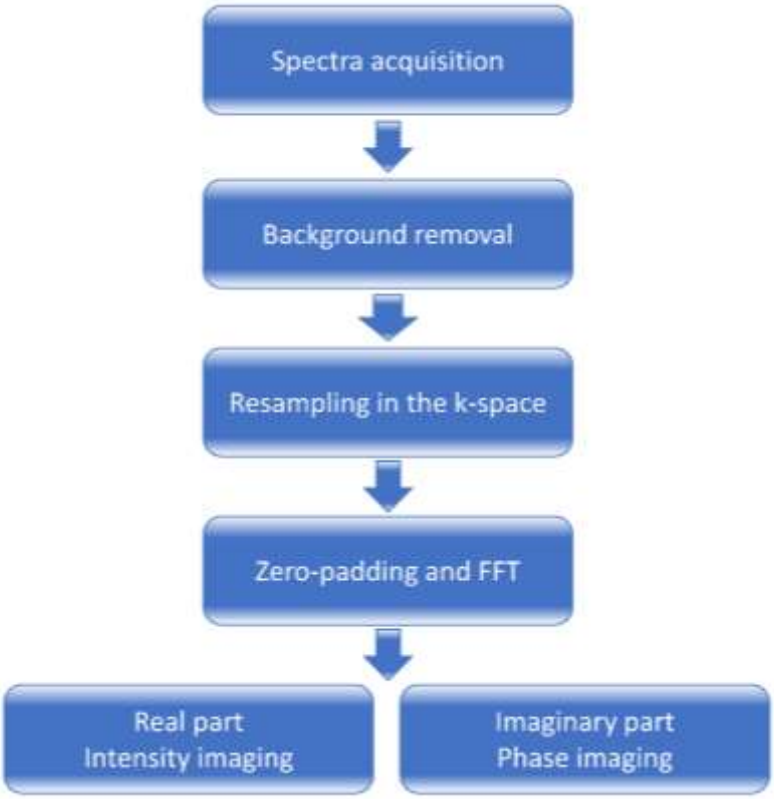

Figure 3: Digital processing of acquired OCPM spectra to retrieve intensity image and phase information at each pixel.

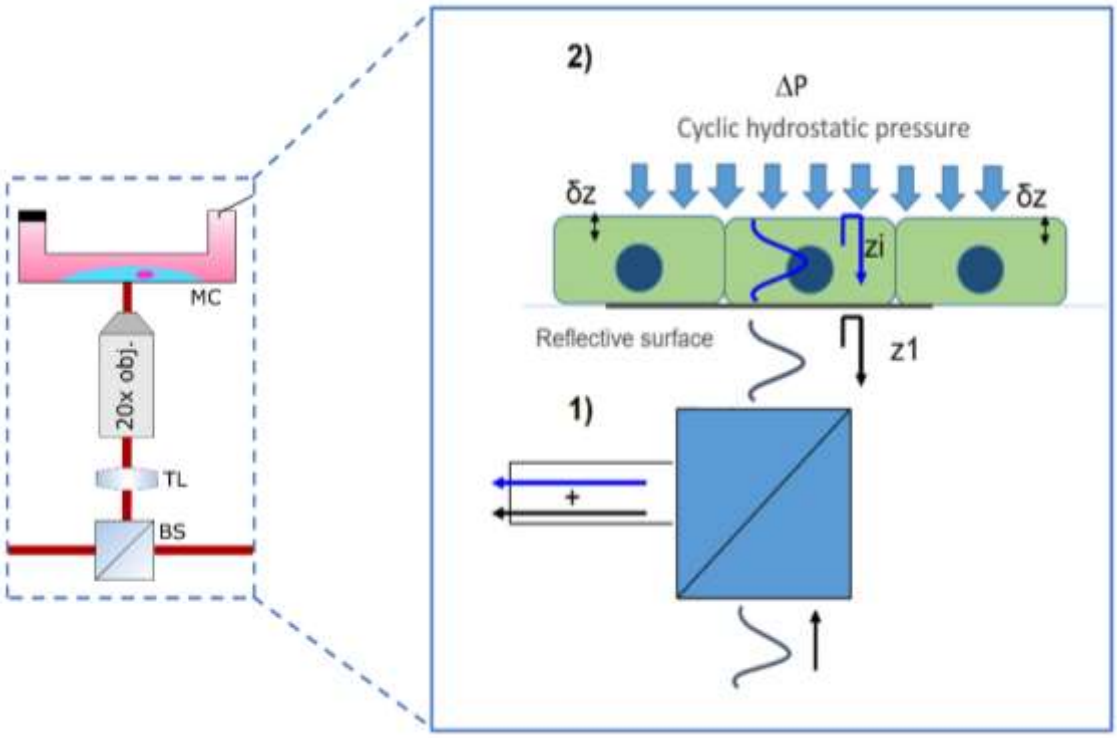

Figure 4: Relative displacement induced by hydrostatic pressure measured as a change in phase. 1) Imaging system 2) Cyclic hydrostatic pressure is applied to cells which are cultured on a clear, reflective surface, which results in a change in the phase signal.

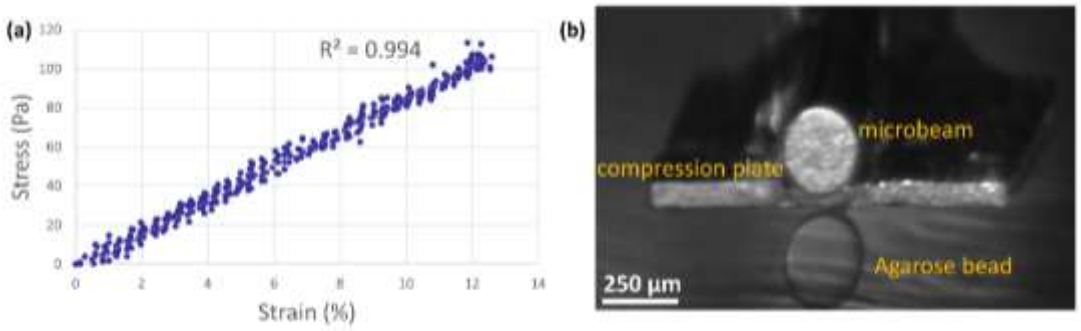

Figure 5: Mechanical properties of 6% agarose beads: Representative stress- strain curve of 350 µm bead (a), and compression testing in a water bath at strain rate of 2.5 μms^{-1} (b).

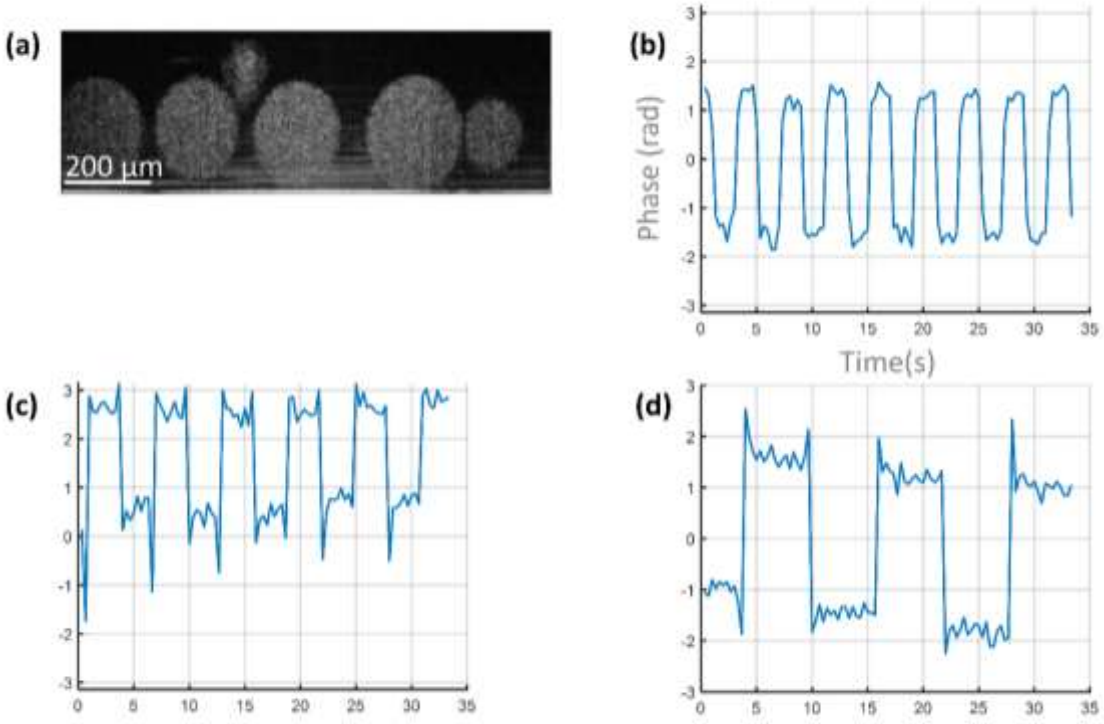

Figure 6: a) OCPM cross section of agarose beads, b-d) response to hydrostatic pressure of 4 s, 6 s, 12 s cycles with 100 mbar amplitude.

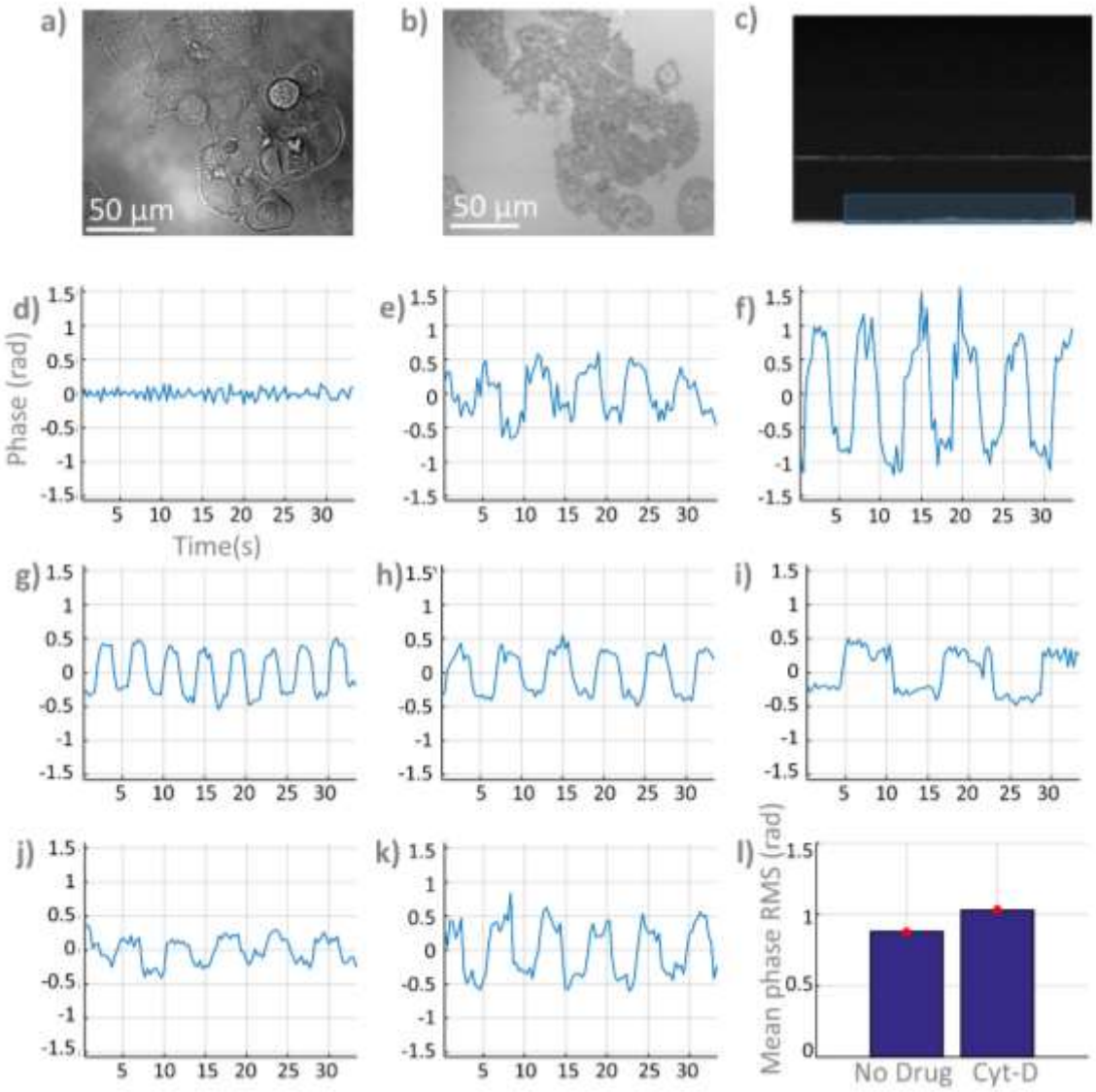

Figure 7: Bright field image (a), OCPM en-face (b), and OCPM 'cell profile' (c) of MCF-7 cells. Cell response at 0, 100, 200 mbar amplitude (d, e, f) with a 6 s cycle, and for various hydrostatic pressure period, 4 s, 6 s,12 s cycles with 200 mbar amplitude (g, h, i), and (j) Typical cell response before drug addition (6 s, 50 mbar) and after addition of 10 µM Cytochalasin-D (k). (l) Mean response (N=242 pixels) shows significant ($p<0.01$) increase in cell response. Phase value was taken at a representative pixel rather than the same pixel location within the cell.

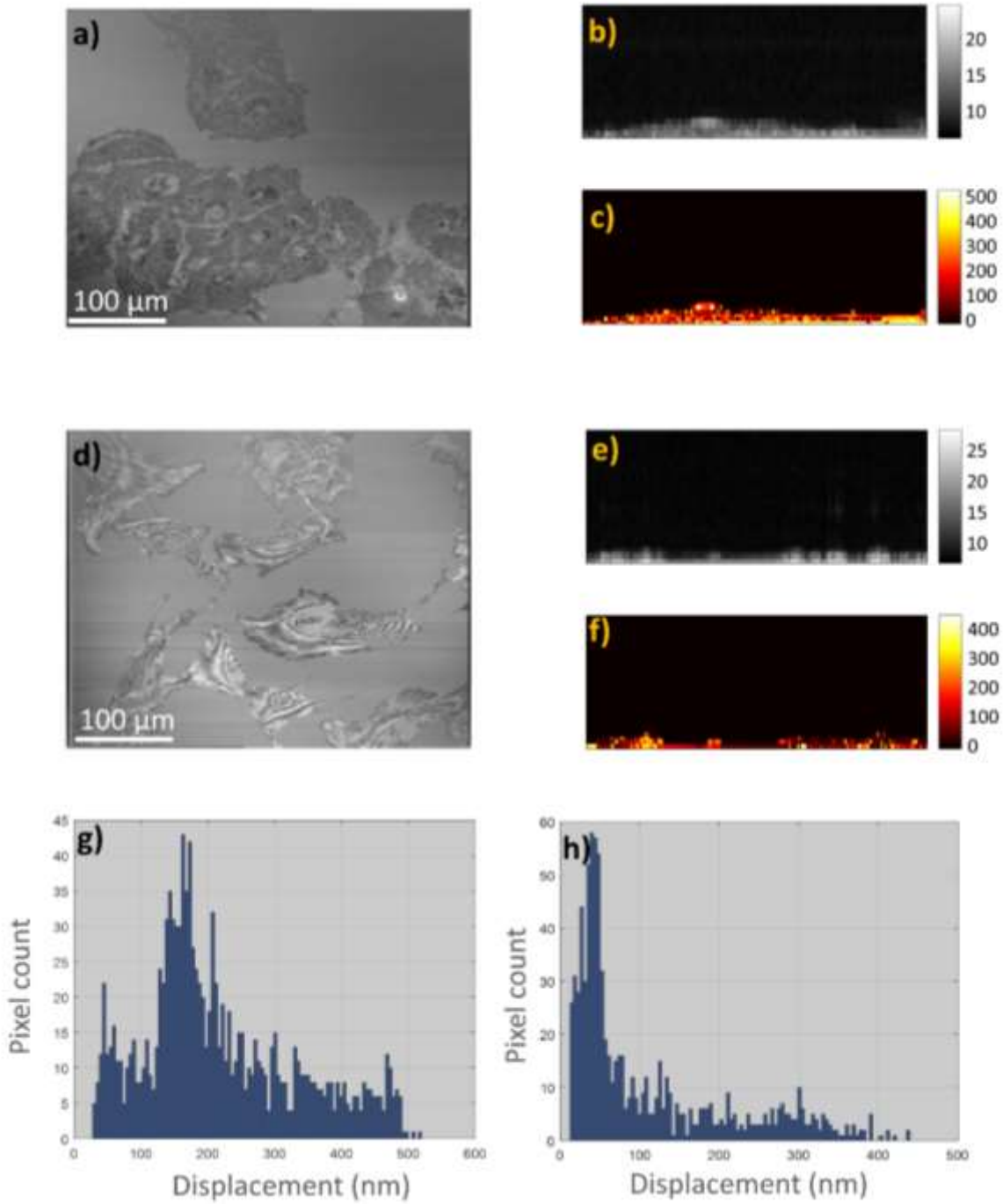

Figure 8: OCPM en-face live imaging of MCF-7 cells (a) and 3T3 cells (d) with typical OCPM cross-section, 'cell profile', (b) and (e) and associated relative cell displacement induced by hydrostatic pressure (c) and (f). Heterogeneity in intracellular displacement was found in histograms of displacement (g, h) with a marked difference between 3T3 and MCF-7 which suggested 3T3 being stiffer.